Supporting Information

Chlorine-mediated construction of monometallic Ru-RuO_2 with abundant interfaces for efficient pH-universal hydrogen evolution catalysis

Jiao Yang[a], Lishan Peng[b*], Youpeng Cao[a], Lun Li[a], Zhichao Yu[a], Chengcheng Zhong[a], Wendi Zhang[a], Weng Fai Ip[c], and Hui Pan[a,c*]

[a] *Institute of Applied Physics and Materials Engineering, University of Macau, Macao SAR, 999078, China*

[b] *Key Laboratory of Rare Earths, Ganjiang Innovation Academy, Chinese Academy of Sciences, Ganzhou 341119, China*

[c] *Department of Physics and Chemistry, Faculty of Science and Technology, University of Macau, Macao SAR, 999078, China*

E-Mail : lspeng@gia.cas.cn; huipan@um.edu.mo

Experimental Sections

Synthesis of the RuOCl catalyst:

In a typical synthesis, 5.0 g of $NaNO_3$ was first placed at the bottom of a 50 mL quartz beaker. This beaker is then transferred to a muffle furnace preheated to 350 °C and heated for 20 minutes to completely melt $NaNO_3$ into a transparent molten salt system. Subsequently, 50 mg of $RuCl_3 \cdot xH_2O$ is rapidly added to the molten $NaNO_3$. After the addition, the mixture is maintained at 350 °C for another 3 minutes; a color change in the melt is observed during this time. Once the reaction is complete, the quartz beaker is removed from the muffle furnace and allowed to cool naturally at room temperature until solidification. After cooling down, 50 mL of deionized (DI) water was added to dissolve $NaNO_3$. The RuOCl nanosheets were collected by centrifugation and washed with DI water 5 times. Finally, the product was re-dispersed in 5 mL of DI water and freeze-dried under vacuum.

Synthesis of the RuO_2 catalyst:

Consistent with the aforementioned method for synthesizing RuOCl, the only difference is that $RuCl_3 \cdot xH_2O$ is replaced by $Ru(acac)_3$.

Synthesis of the Ru/RuO_2 catalyst:

To obtain Ru/RuO_2, the as-prepared RuOCl catalyst was further annealed at 120 °C for 30min in a hydrogen atmosphere, with a heating rate of 5℃/min. which was denoted as Ru/RuO_2.

Synthesis of the $Ru@RuO_2$ catalyst:

Typically, 100mg of commercial RuO_2 was placed in a porcelain boat, further annealed at 120 °C for 30min with a heating rate of 5℃/min in a hydrogen atmosphere, and the obtained sample was donated as $Ru@RuO_2$.

Synthesis of the pristine Ru catalyst:

To obtain Ru, the as-prepared RuO_2 catalyst was further annealed at 200 °C for 2h

with a heating rate of 5℃/min in a hydrogen atmosphere, which was denoted as Ru.

Material characterizations

Phase identification was performed by X-ray diffraction (XRD) analysis. The XRD patterns were obtained from a Rigaku SmartLab SE diffractometer by scanning the angular range $5° \leq 2\theta \leq 90°$ using Cu Kα radiation (λ = 1.5418 Å). X-ray photoelectron spectroscopy (XPS) was obtained using a Thermo Scientific Escalab 250Xi spectrometer. The morphology and microstructure were evaluated using transmission electron microscopy (TEM, JEM2010-HR). Raman spectra were recorded with a LABHRev-UV Raman spectrometer ranging from 200 to 1000 cm^{-1}. Inductively coupled plasma-optical emission spectroscopy (ICP-OES, Varian 710) was used to quantify the amount of Ru in the samples. To prepare the samples for ICP-OES, the samples were placed in the hydrothermal reaction vessel, using nitric acid as the solvent, to ensure that the Ru element is fully dissolved. Then, place the reaction vessel in the muffle furnace and let it react at 60 ℃ for 3 hours. Finally, the solutions were diluted to the ppm range for the ICP-OES measurements.

Electrochemical characterization

Electrochemical measurements were performed at room temperature using a rotating disk electrode (DC DSR，PHYCHEMI) made of glassy carbon (GC, 0.196 cm^2) connected to a CHI 760E electrochemistry workstation (Shanghai Chenhua Instruments Company, Shanghai, China). The GC electrode was fully polished and thoroughly cleaned before use. The Hg/HgO electrode was used as a reference electrode in alkaline solution, while the Hg/Hg_2SO_4 electrode was used as a reference electrode for acidic and neutral electrolytes tests. The polarization curves were tested in 1 M KOH, 0.5 M H_2SO_4, and 1 M PBS, respectively, with a sweep rate of 10 mV/s. All the

measured potentials were converted to a reversible hydrogen electrode (RHE).

The working electrode was prepared as follows. In short, 3 mg of electrocatalyst powder was dispersed in 970 μl iso-propanol mixed solvent with 30 μL of Nafion solution (5 wt%, Sigma-Aldrich), and then the mixture was ultrasonicated for about 1 hour to generate a homogeneous ink. Next, 10 μL of the dispersion was transferred onto the GC disk, leading to the electrocatalyst loading of ~0.15 mg cm^{-2}. Finally, the as-prepared electrocatalyst film was dried at room temperature. Meanwhile, 3 mg of 20% Pt/C (Aladdin Industrial Corporation) was dispersed in 970 μL of isopropanol, and 30 μL of Nafion (5 wt%, Sigma-Aldrich) solution, and then 10 μL of the solution was dropped onto a glassy carbon electrode to achieve a catalyst loading of ~0.15 mg cm^{-2}.

The electrochemical surface active area (ECSA) of the samples were estimated from double-layer capacitance (C_{dl}) and specific capacitance (C_s) using the following equation.

$$ECSA\ (m^2g^{-1}) = C_{dl}/(Cs \times m)$$

where C_{dl} is the measured double-layer capacitance (mF) from the CV curves in the non-faradaic region, m is the mass loading of the electrocatalyst (g), and C_s is the specific capacitance of the sample or the capacitance of an atomically smooth planar surface of the material per unit area under identical electrolyte conditions. We used general specific capacitances of C_s = 0.035 mF cm^{-2} based on the typically reported value. Electrochemical impedance spectroscopy (EIS) of the electrode was measured at 1.6 V *vs.* RHE with an amplitude of 5 mV over a frequency range of 0.01–100000 Hz.

Computational Details

DFT calculations were conducted on the projector-augmented wave (PAW) [1] in

the Vienna Ab initio Simulation Package (VASP) [2]. The generalized gradient approximation (GGA) of Perdew-Burke-Ernzerhof (PBE) [3] exchange functional was applied. The cut-off energy for the plane-wave basis was set as 450 eV. A 20 Å vacuum slab in a direction perpendicular to the surface of the catalyst was adopted to avoid periodic interactions. The Brillouin zone integration was performed with 3 × 3 × 1 Monkhorst–Pack k-point sampling for geometry relaxation [4]. For the calculation of DOS, the k-point mesh was increased to 6 × 6 × 1. The convergence threshold for force and energy during optimization was set as 0.03 eV/Å, and 10^{-4} eV, respectively. The climbing image nudged elastic band method (CI-NEB) was used to identify the water decomposition and hydrogen spillover pathway. The geometry structures and charge density difference plots were illustrated with VESTA software.

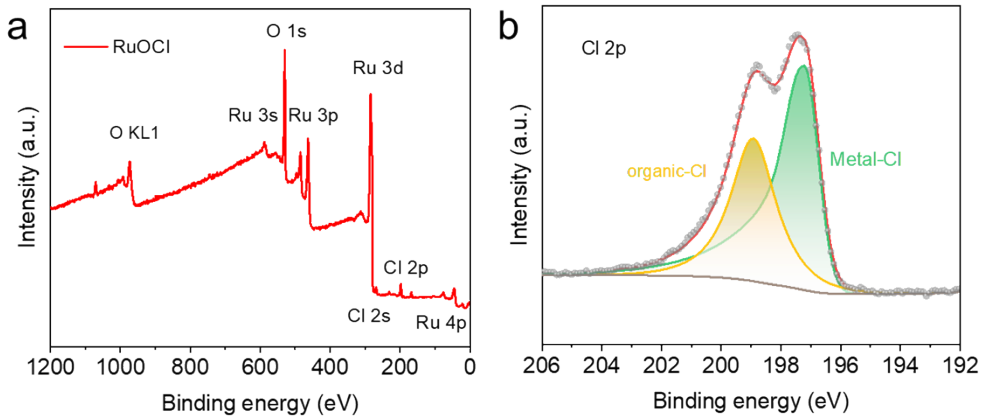

Figure S1. (a) XPS survey spectra of RuOCl. (b) Cl 2p XPS of RuOCl.

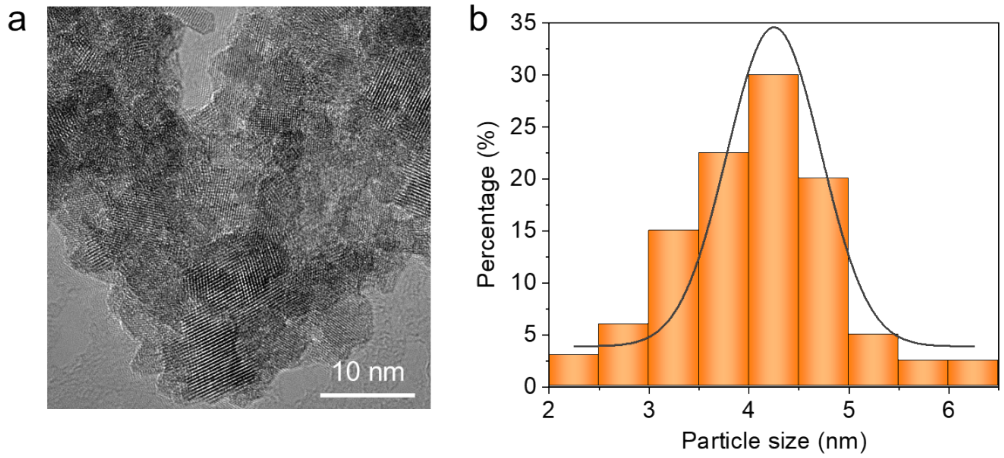

Figure S2. TEM image of the Ru/RuO_2, and (b) Histogram of the particle sizes.

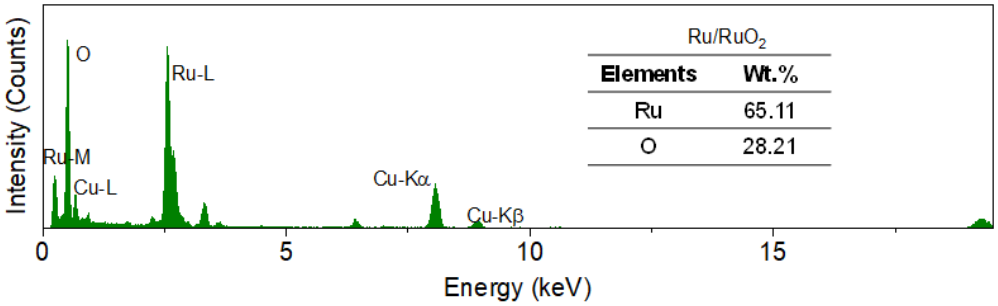

Figure S3. EDX spectrum of Ru/RuO_2.

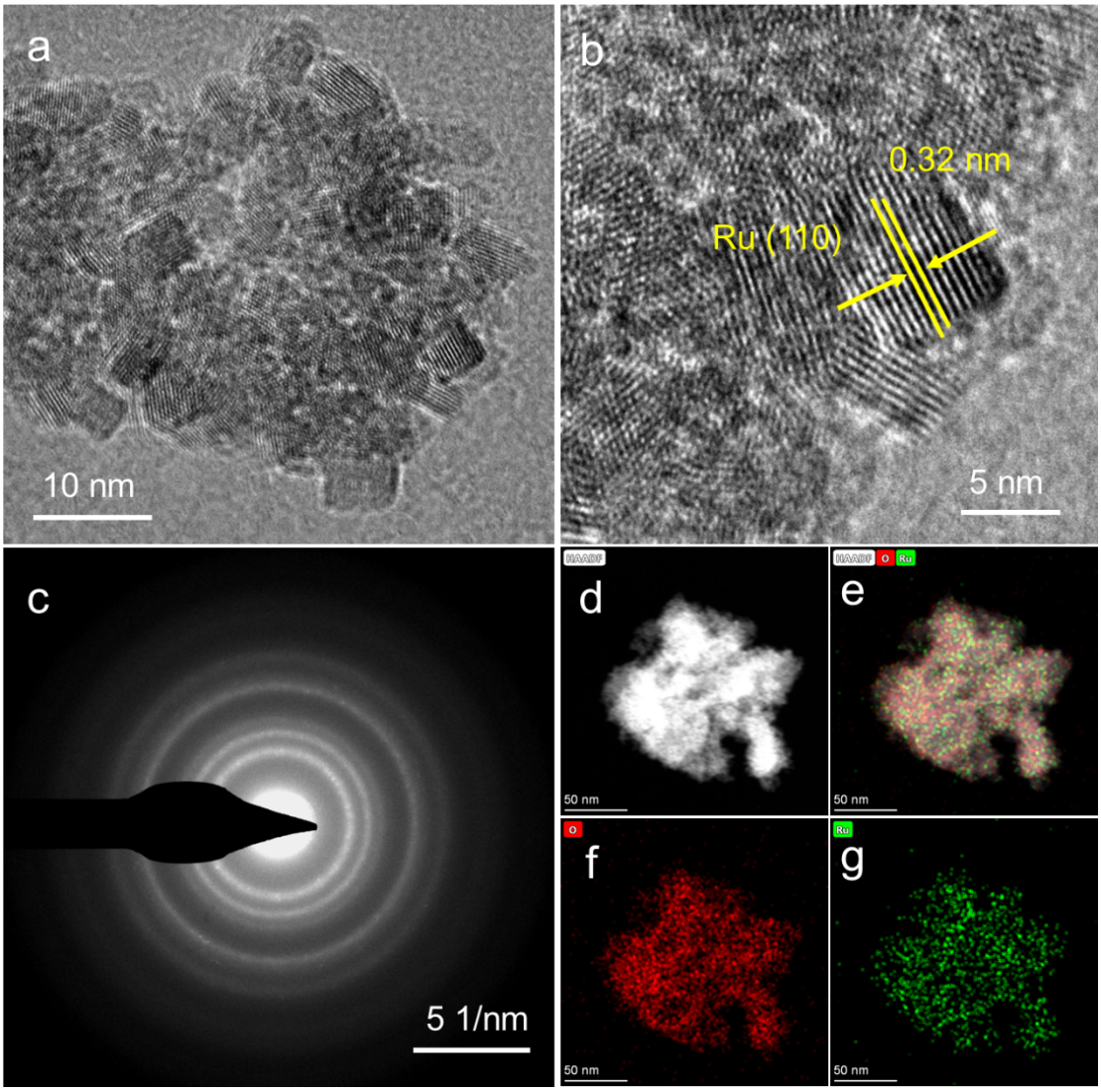

Figure S4. The morphology and microstructure of RuO_2. (a) TEM image, (b) The enlarged TEM image, (c) SAED pattern, and (d-g) Element mapping.

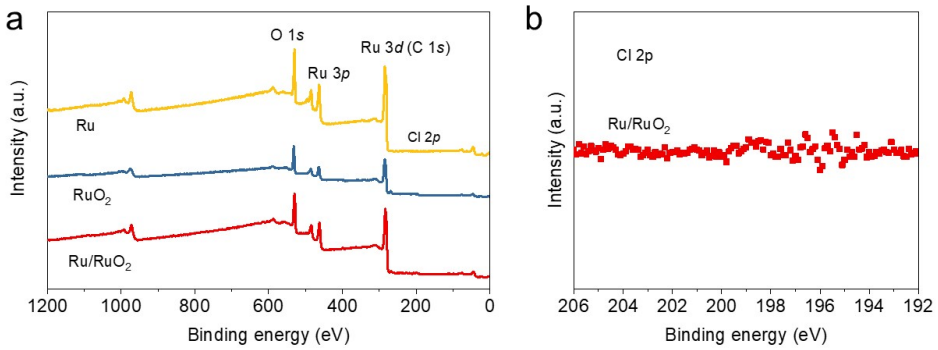

Figure S5. (a) XPS survey spectra of Ru, RuO_2, and Ru/RuO_2. (b) Cl 2p XPS spectrum of the Ru/RuO_2 sample.

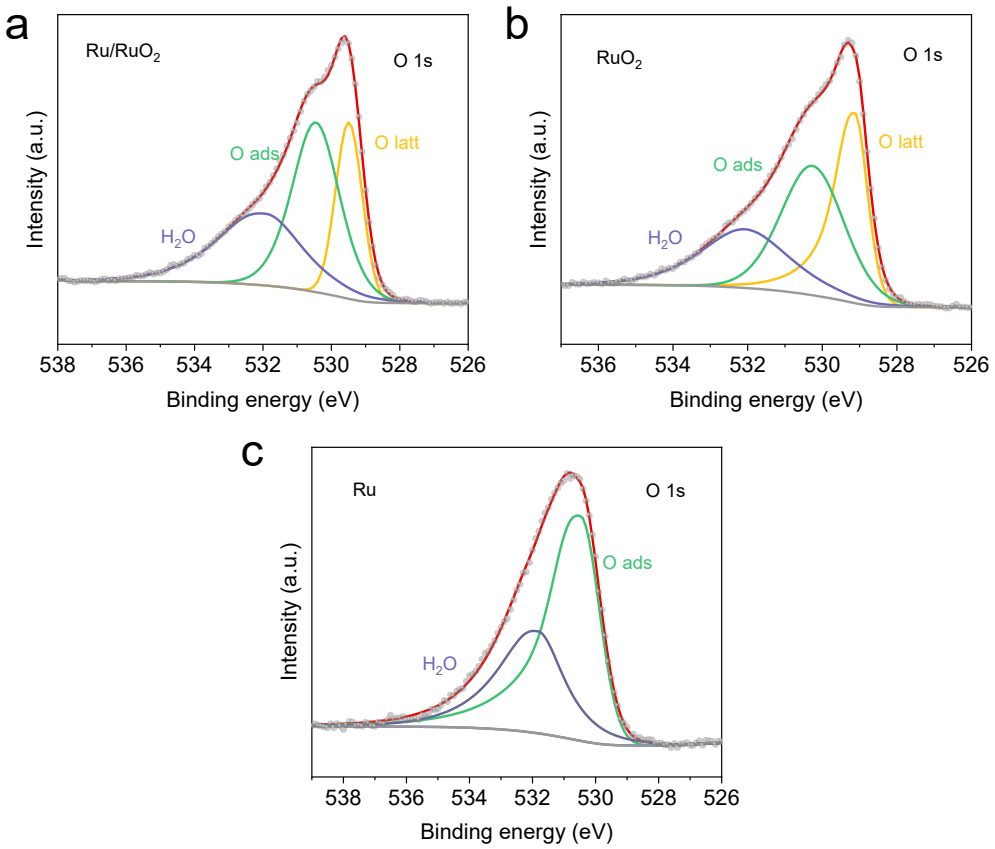

Figure S6. XPS survey spectra of O1s for (a-c) Ru, RuO_2, and Ru/RuO_2.

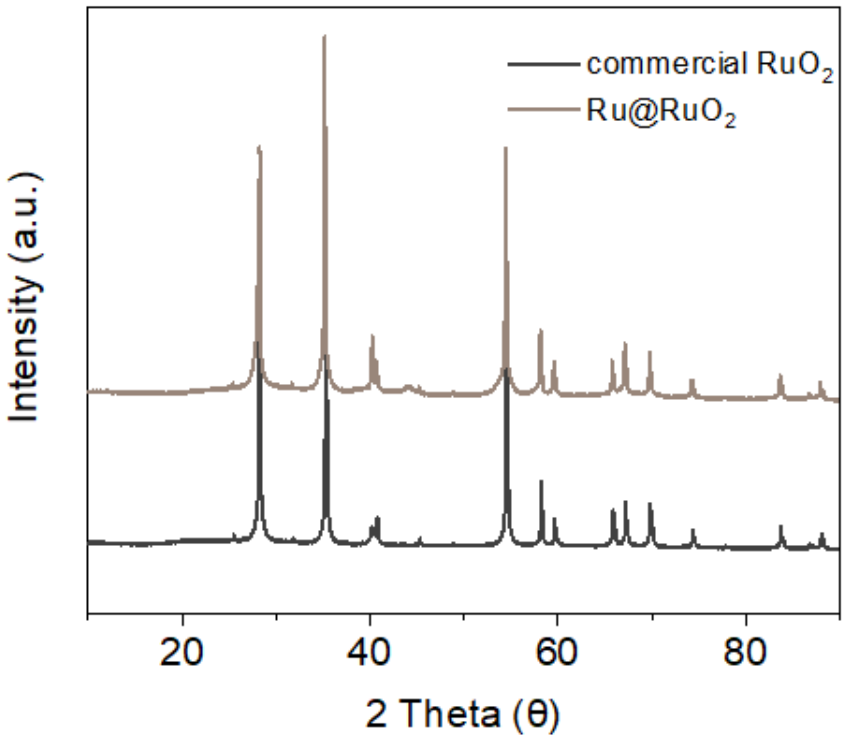

Figure S7. XRD pattern of commercial RuO_2 and $Ru@RuO_2$.

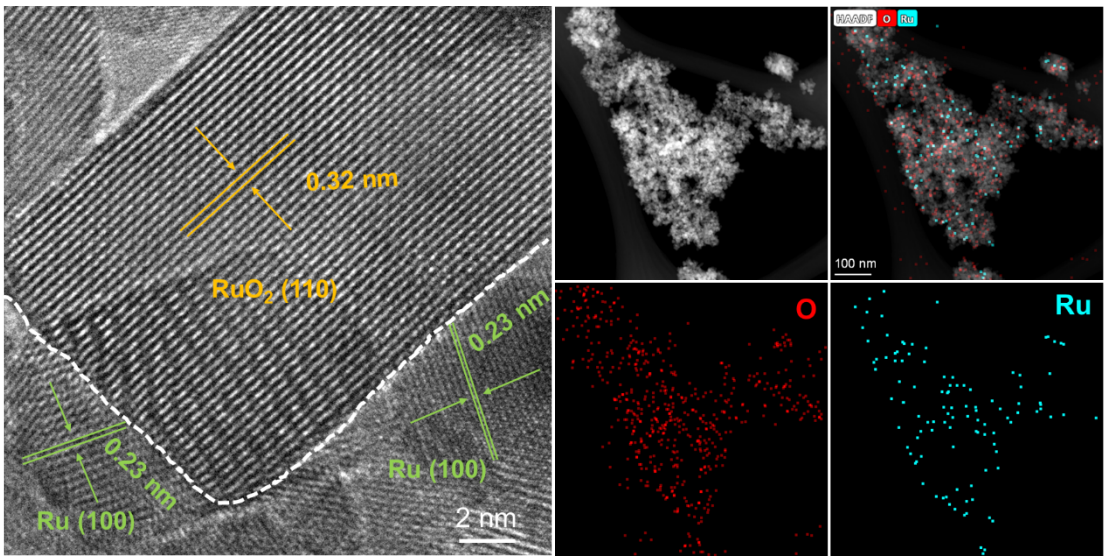

Figure S8. The morphology and microstructure of Ru@RuO_2.

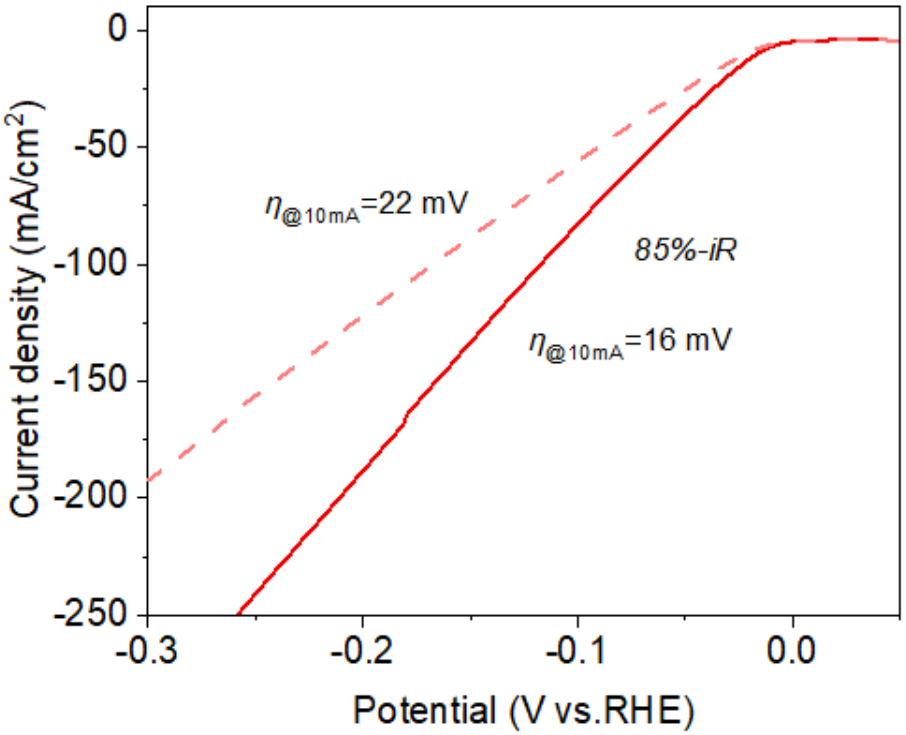

Figure S9. HER performance of Ru/RuO_2 in M KOH with and without IR correction.

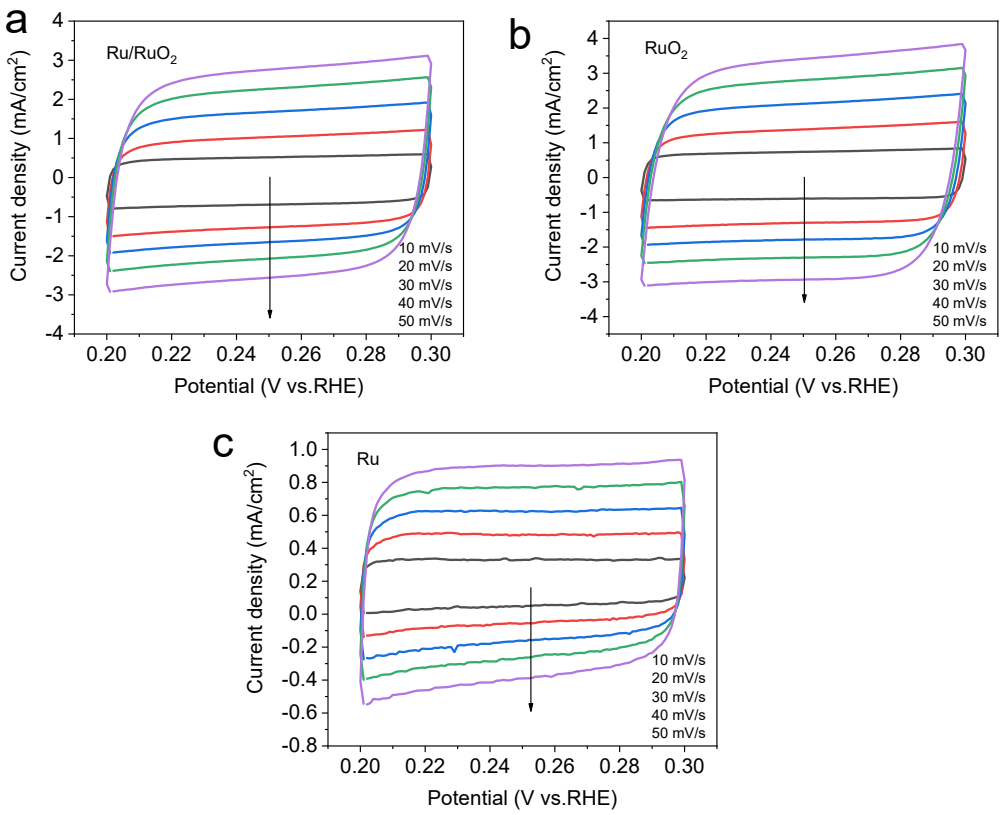

Figure S10. Cyclic voltammetric profiles of (a) Ru/RuO_2, (b) RuO_2, (c) Ru electrodes measured at different scan rates in the potential range of 0.2-0.3 V (vs. RHE).

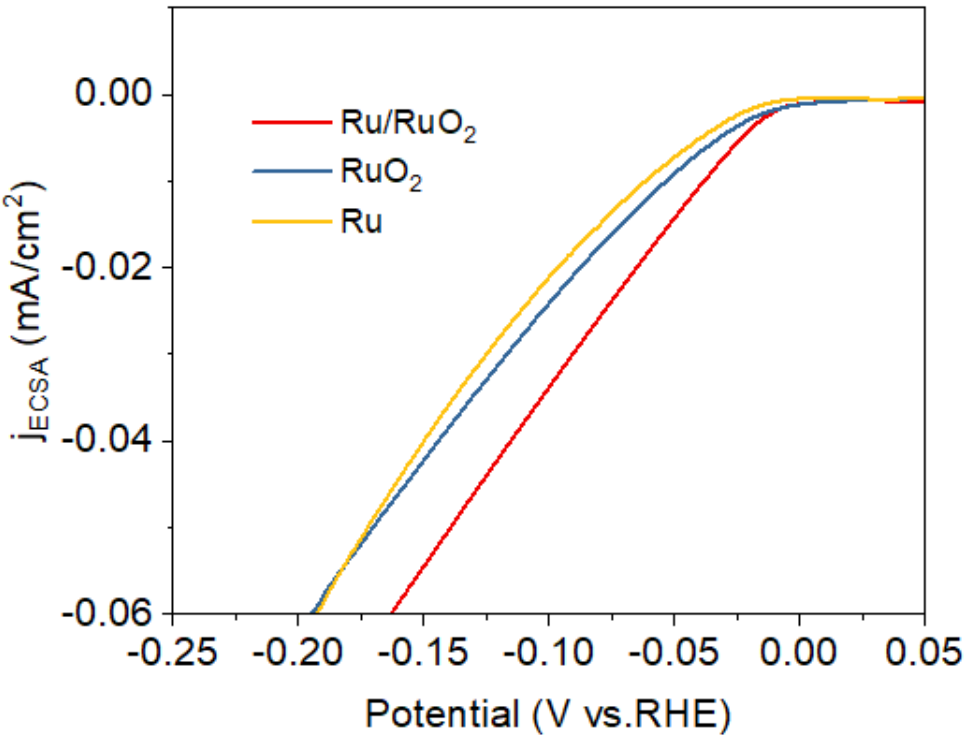

Figure S11. Relative ECSA normalized LSV curves of Ru/RuO_2, RuO_2, and Ru catalysts in 1 M KOH electrolyte.

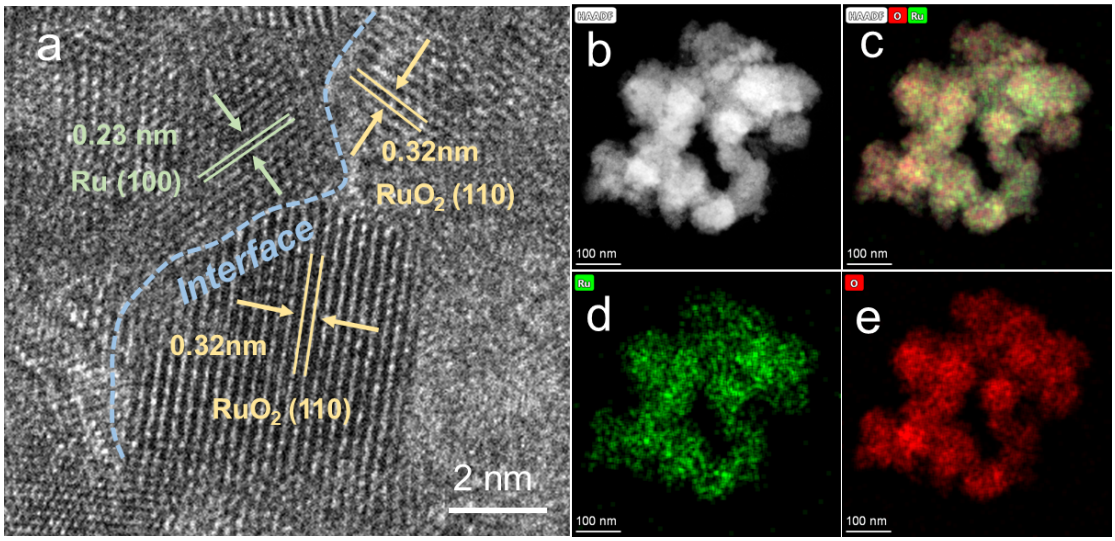

Figure S12. (a) HRTEM image, (b-e) Element mapping of Ru/RuO_2 after HER test in 1 M KOH electrolyte.

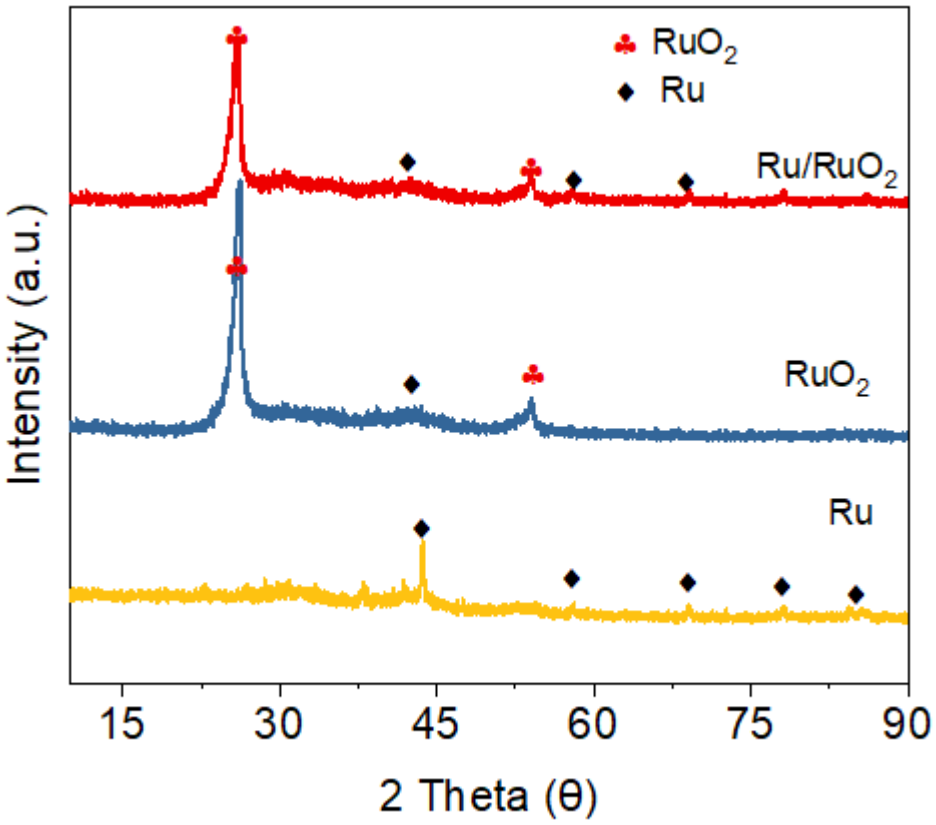

Figure S13. Post-mortem tests of Ru/RuO_2 after HER stability test in 1 M KOH electrolyte.

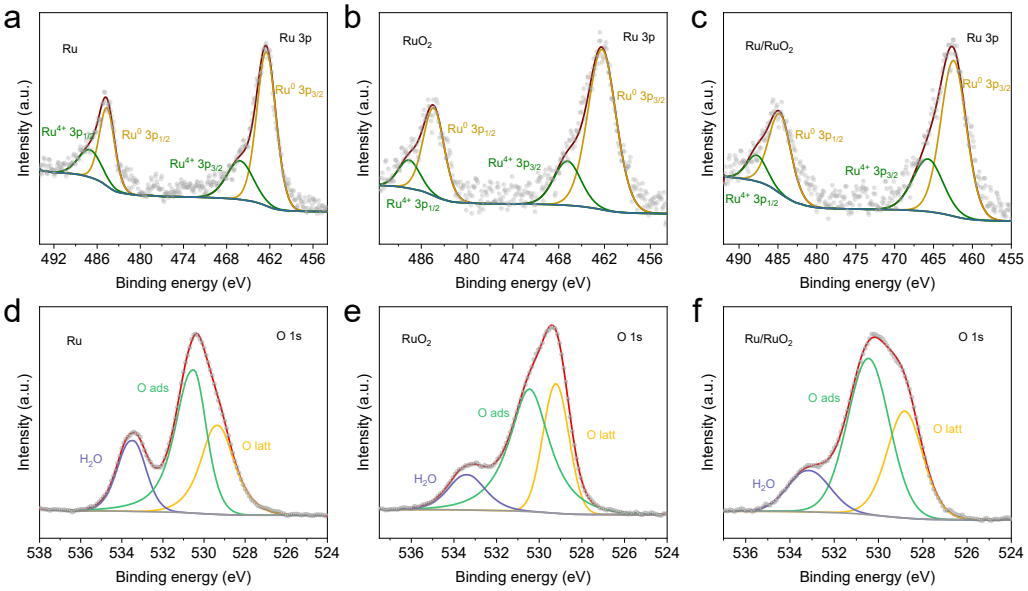

Figure S14. (a-c) Ru 3p, (d-f) O 1s XPS spectra of Ru, RuO_2, and Ru/RuO_2 after HER reaction.

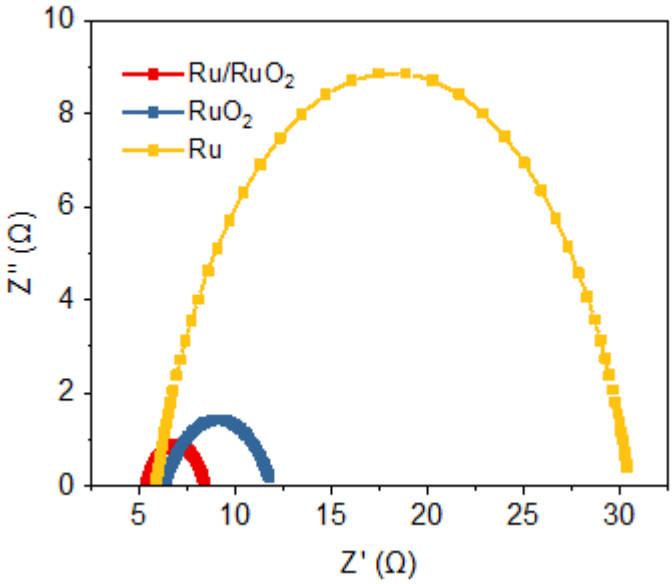

Figure S15. Electrochemical impedance spectroscopy of the synthesized samples in 0.5M H_2SO_4.

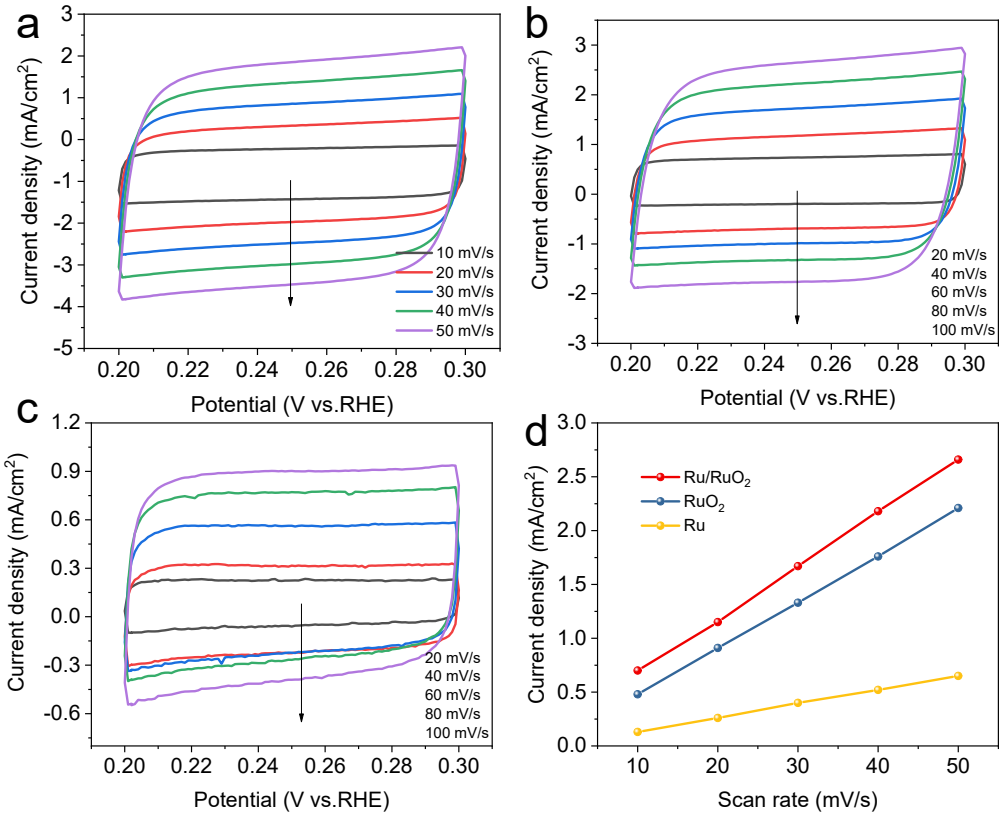

Figure S16. (a-c) CV profiles of Ru/RuO_2, RuO_2, and Ru. (d) The double-layer capacitance in 0.5 M H_2SO_4.

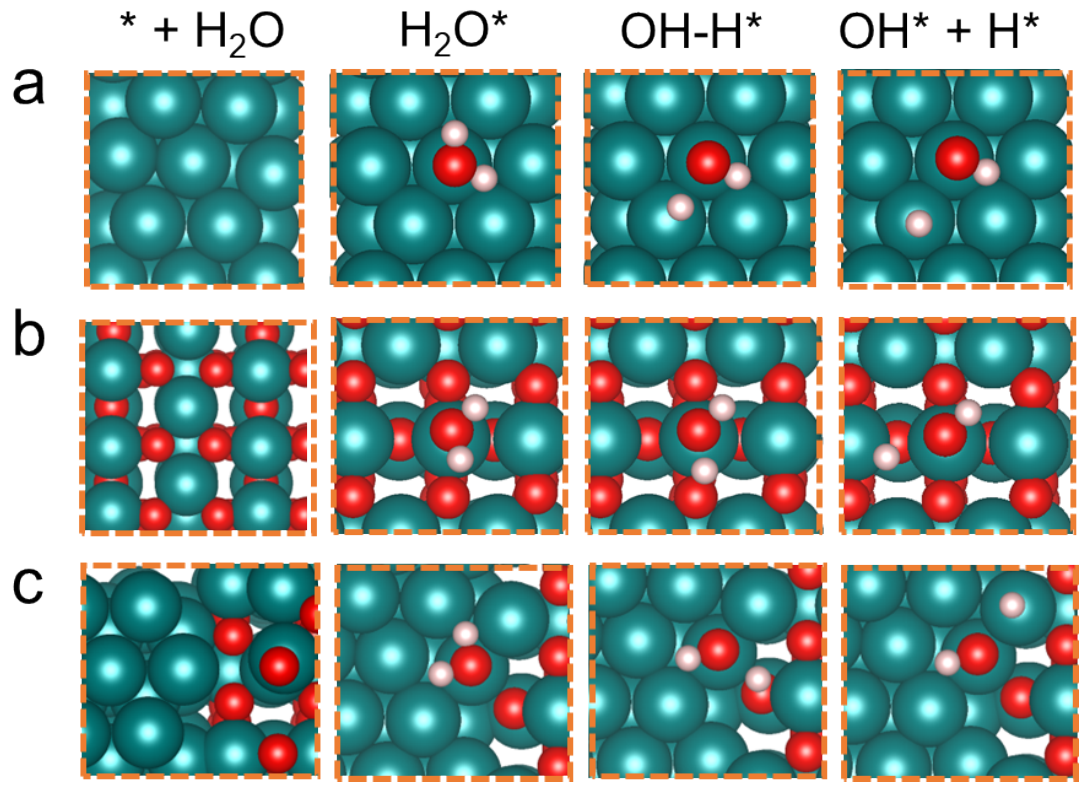

Figure S17. Water adsorption and dissociation configuration diagram of * + H_2O, H_2O*, OH-H*, and OH* + H* on the (a) Ru (110), (b) RuO_2, and (c) Ru/RuO_2. The cyan, red, and pink represent Ru, O, and H elements, respectively.

Table S1. Ru contents were measured by ICP-OES for Ru, RuO_2, and Ru/RuO_2.

Catalyst	**Ru content (wt.%)**
Ru	98.2
RuO_2	69.4
Ru/RuO_2	77.1

Table S2. HER performance comparison of Ru/RuO_2 with that of most recently reported Ru-based HER electrocatalysts in 1 M KOH.

Catalyst	η (mV) at 10 mA/cm²	Tafel slope (mV/dec)	Ref.
NiO/Ru@Ni	39	75	[5]
RuP_x@NPC	74	70	[6]
HP-Ru/C	25	29	[7]
Ru-Ru_2P/PC	43.4	35.1	[8]
Ru@CN-0.16	32	53	[9]
Ru-Mo_2C-CN	34	80	[10]
Ru/NC-400	39	49	[11]
Pd-Ru@NG	28	73	[12]
Ru-MoS_2-Mo_2C-TiN	25	58	[12]
RuP_2@NPC	52	69	[14]
Ru-MoO_2	29	31	[15]
Ru-NGC	37	40	[16]
SA-Ru-MoS_2	76	21	[17]

Table S3. Comparison of the HER activity of Ru/RuO_2 with that of recently reported noble metal-based electrocatalysts in neutral media.

Catalyst	η (mV) at 10 mA/cm²	Tafel slope (mV/dec)	Ref.
Ru-Cr_2O_3/NG	53	47	[18]
PdP_2@CB	86.4	72.3	[19]
Ru/MeOH/THF	83	-	[20]
Pt-$Co(OH)_2$/CC	32	70	[21]
RuNi/CQDs	18	76	[22]
Rh_2P	38	46	[23]
10% wt Ir/$W_{18}O_{49}$	83	66	[24]
Ru-WO_{3-x}/CP	19	41	[25]

Table S4. Comparison of the HER activity of Ru/RuO_2 with that of recently reported noble metal-based electrocatalysts in acidic electrolyte.

Catalyst	η (mV) at 10 mA/cm^2	Tafel slope (mV/dec)	Ref.
Ru-Cr_2O_3/NG	53	47	[18]
PdP_2@CB	86.4	72.3	[19]
Ru@Co/N-CNTs	92	73	[21]
Rh@CTF-1	58	37	[26]
RuNi/CQDs	58	55	[22]
Ru_2P	101	-	[27]
MoP-Ru_2P/NPC	82	65	[28]
$RuTe_2$/Gr	72	33	[29]
ECM@Ru	63	47	[30]

Table S5. Comparison of the mass activity of Ru/RuO_2 with that of reported Ru-based electrocatalysts.

Catalyst	Mass activity	Test condition	Ref.
Ru/RuO_2	4.93 A $mgRu^{-1}$ @ 100 mV	1 M KOH	**This work**
Ru/RuO_2 SNSs	9.13 A $mgRu^{-1}$ @ 50 mV	0.1 M KOH	*Sci. Bull. 67.20 (**2022**): 2103-2111*
Ru SA/Co_3O_4	4.7 A $mgRu^{-1}$ @ 50 mV	1 M KOH	*ACS nano 19.11 (**2025**): 11176-11186*
Ru-NiO/CNTs	1.83 A $mgRu^{-1}$@ 100 mV	1 M KOH	*Chem. Eng. J. 472 (**2023**): 144922*
Ru-GaSA/N-C	9.3 A $mgRu^{-1}$ @ η=50 mV	1 M KOH	*Nat. Commun. 15.1 (**2024**): 6741*
Ru-V_8C_7/C	1.9 A $mgRu^{-1}$ @ 40 mV	1 M KOH	*Sci. Bull. 69.6 (**2024**): 763-771*
Rux@NOH/NO	18.8 A $mgRu^{-1}$@ 150 mV	1 M KOH	*Electrochim. Acta 505 (**2024**): 144953*
Ru/Mo_2N	1.71 A $mgRu^{-1}$@ 100 mV	1 M KOH	Chin. Chem. Lett. 36.4 (2025): 109845

Reference:

[1] Blöchl P E. Phys. Rev. B, 1994, 50, 17953.

[2] Kresse G, Furthmüller J., J. c. Phys. Rev. B, 1996, 54, 11169.

[3] Perdew J P, Burke K, Ernzerhof M. Phys. Rev. Lett., 1996, 77, 3865.

[4] Weiler M H, Aggarwal R L, Lax B. Phys. Rev. B, 1977, 16, 3603.

[5] C. Zhong, Q. Zhou, S. Li, L. Cao, J. Li, Z. Shen, H. Ma, J. Liu, M. Lu, H. Zhang, J. Mater. Chem. A. 2019, 7, 2344.

[6] J. Chi, W. Gao, J. Lin, B. Dong, ChemSusChem. 2018, 11, 743.

[7] C. B. Hong, X. Li, W. B. Wei, X. T. Wu, Q. L. Zhu, Appl. Catal., B. 2021, 294, 120230.

[8] Z. Pu, I. S. Amiinu, Z. Kou, W. Li, S. Mu, Angew. Chem., Int. Ed. 2017, 56, 11559.

[9] J. Wang, Z. Wei, S. J. Mao, H. Li, Y. Wang, Energy Environ. Sci. 2018, 11, 1.

[10] J. Chen, C. Chen, Y. Chen, H. Wang, S. Mao, Y. Wang, J. Catal. 2020, 392, 313.

[11] M. Lao, G. Zhao, P. Li, T. Ma, Y. Jiang, H. Pan, S. X. Dou, W. Sun, Adv. Funct. Mater. 2021, 31, 2100698.

[12] B. K. Barman, B. Sarkar, K. K. Nanda, Chem. Commun. 2019, 55, 13928.

[13] V. H. Hoa, D. T. Tran, S. Prabhakaran, D. H. Kim, J. H. Lee, Nano Energy. 2021, 88, 106277.

[14] Z. Pu, I. S. Amiinu, Z. Kou, W. Li, S. Mu, Angew. Chem., Int. Ed. 2017, 56, 11559.

[15] J. Peng, Y. Yang, R. Shi, G. Xia, Q. Chen, J. Mater. Chem. A. 2017, 5, 5475.

[16] S. Qian, X. Qiao, L. Liu, Z. Xue, C. Huang, Chem. Commun. 2019, 55, 965.

[17] J. Zhang, X. Xu, L. Yang, D. Cheng, D. Cao, Small Methods. 2019, 3, 1900653.

[18] L. Tang, J. Yu, Y. Zhang, Z. Tang, Y. Qin, RSC Adv. 2021, 11, 6107.

[19] F. Luo, Q. Zhang, X. Yu, S. Xiao, Y. Ling, H. Hu, L. Guo, Z. Yang, L. Huang, W. Cai, H. Cheng, Angew. Chem., Int. Ed. 2018, 57, 14862.

[20] S. Drouet, J. Creus, V. Colliere, C. Amiens, J. Garcia-Anton, X. Sala, K. Philippot,

Chem Commun (Camb). 2017, 53, 11713.

[21] Z. Xing, C. Han, D. Wang, Q. Li, X. Yang, ACS Catal. 2017, 7, 7131.

[22] Y. Liu, X. Li, Q. Zhang, W. Li, Y. Xie, H. Liu, L. Shang, Z. Liu, Z. Chen, L. Gu, Z. Tang, T. Zhang, S. Lu, Angew Chem Int Ed Engl. 2020, 59, 1718.

[23] F. Yang, Y. Zhao, Y. Du, Y. Chen, G. Cheng, S. Chen, W. Luo, Adv. Energy Mater.

2018, 8, 1703489.

[24] C. Peng, W. Zhao, Z. Kuang, J. T. Miller, H. Chen, Appl. Catal. A. 2021, 623, 118293.

[25] J. Chen, C. Chen, M. Qin, B. Li, B. Lin, Q. Mao, H. Yang, B. Liu, Y. Wang, Nat Commun. 2022, 13, 5382.

[26] M. Siebels, C. Schlüsener, J. Thomas, Y.-X. Xiao, X.-Y. Yang, C. Janiak, J. Mater. Chem. A. 2019, 7, 11934.16

[27] Y. Li, F. Chu, Y. Bu, Y. Kong, Y. Tao, X. Zhou, H. Yu, J. Yu, L. Tang, Y. Qin, Chem.

Commun. 2019, 55, 7828.

[28] Y. Gao, Z. Chen, Y. Zhao, W. Yu, X. Jiang, M. He, Z. Li, T. Ma, Z. Wu, L. Wang, Appl. Catal., B. 2022, 303, 120879.

[29] X. Gu, X. Yang, L. Feng, Chemistry – An Asian Journal. 2020, 15, 2886.

[30] H. Zhang, W. Zhou, X. F. Lu, T. Chen, X. W. Lou, Adv. Energy Mater. 2020, 10, 2000882.